Available online at www.sciencedirect.com

ScienceDirect

Ceramics International 39 (2013) 9309–9317

CERAMICS INTERNATIONAL

www.elsevier.com/locate/ceramint

Electrochemical behaviors of hexagonal $LiMnBO_3$ as lithium storage host material for lithium-ion batteries

Rui Ma, Lianyi Shao, Kaiqiang Wu, Mengmeng Lao, Miao Shui, Cheng Chen, Dongjie Wang, Nengbing Long, Yuanlong Ren, Jie Shu*

Faculty of Materials Science and Chemical Engineering, Ningbo University, Ningbo 315211, Zhejiang Province, People's Republic of China

Received 20 April 2013; received in revised form 14 May 2013; accepted 15 May 2013
Available online 21 May 2013

Abstract

Hexagonal $LiMnBO_3$ samples with particle size bewteen 0.2 and 1.0 μm are prepared by a carbothermal reaction using stoichiometric mixture of $LiOH \cdot H_2O$, $Mn(CH_3COO)_2 \cdot 4H_2O$, H_3BO_3 and carbon black as starting materials. Powder X-ray diffraction and infrared studies of the as-prepared products indicate that hexagonal $LiMnBO_3$ with space group of P-6 is formed under high temperature calcination at 750 °C. Electrochemical study shows that hexagonal $LiMnBO_3$ as cathode material for lithium-ion batteries can deliver an initial charge capacity of 148.4 m Ah g^{-1} (0.668 Li) in the potential range 2.5–4.8 V, corresponding to the delithiation plateau at 4.76 V. Combined with the charge–discharge curves, ex-situ structural investigations show that the delithiation–lithiation mechanism of hexagonal $LiMnBO_3$ cathode is associated with a two-phase transformation reaction. In contrast, hexagonal $LiMnBO_3$ as anode material for lithium-ion batteries shows a specific discharge capacity of 678.3 m Ah g^{-1} and corresponding specific charge capacity of 353.9 m Ah g^{-1} in the potential range 0.0–3.0 V. After 20 cycles, the reversible charge capacity for hexagonal $LiMnBO_3$ anode is 286.4 m Ah g^{-1} with the capacity retention of 80.9%. The excellent cycling performance is attributed to the quasi-reversible structural evolution as confirmed by ex-situ studies.

Keywords: Hexagonal $LiMnBO_3$; Lithium storage behavior; Cathode material; Anode material; Lithium-ion batteries

1. Introduction

Since the pioneering commercialization on lithium-ion batteries by Sony Corporation in 1991, plenty of efforts have been made on the development of advanced lithium storage materials to replace $LiCoO_2$ as cathode materials in lithium-ion batteries. At the present, lithium-containing transition metal polyoxanion compounds are recognized as attractive alternatives to replace commercial $LiCoO_2$ cathode material owing to their high abundance, low toxicity, better structural and thermal stability. Among the reported lithium-containing transition metal polyoxanion compounds with polyoxanion groups $(XO_m)^{n-}$, such as $(SO_4)^{2-}$, $(AsO_4)^{2-}$, $(MoO_4)^{2-}$, $(WO_4)^{2-}$, $(PO_4)^{3-}$, $(SiO_4)^{3-}$, $(AsO_4)^{3-}$, $(VO_4)^{3-}$ and $(WO_4)^{3-}$, $LiMPO_4$ (M=Fe, Mn) have been promoted as the most promising lithium storage material with strong P–O covalent bonds in the tetrahedral $(PO_4)^{3-}$ ployoxanions building robust host structure and inhibiting oxygen release upon delithiation [1–5]. However, $(PO_4)^{3-}$ polyoxanions having big molecule mass decrease the specific capacity, volumetric and gravimetric energy density of the compound compared to layered cathode materials ($LiMO_2$, M=Fe, Mn, Co, Ni). Therefore, it is necessary to develop novel cathode materials to meet the requirement of high capacity lithium-ion batteries.

Based on our knowledge, it is known that triangle $(BO_3)^{3-}$ polyoxanions show lighter mass than that of the ever reported $(SO_4)^{2-}$, $(AsO_4)^{2-}$, $(MoO_4)^{2-}$, $(WO_4)^{2-}$, $(PO_4)^{3-}$, $(SiO_4)^{3-}$, $(AsO_4)^{3-}$, $(VO_4)^{3-}$ and $(WO_4)^{3-}$ groups. As a result, $LiMBO_3$ (M=Fe, Mn) can show a theoretical capacity of 220 m Ah g^{-1}, which is much higher than that (170 m Ah g^{-1}) of $LiMPO_4$ [6–10]. Moreover, $(BO_3)^{3-}$ polyoxanion compounds display

*Corresponding author. Tel.: +86 574 87600787; fax: +86 574 87609987.
E-mail addresses: shujie@nbu.edu.cn, sergio_shu@hotmail.com (J. Shu).

0272-8842/$ - see front matter © 2013 Elsevier Ltd and Techna Group S.r.l. All rights reserved.
http://dx.doi.org/10.1016/j.ceramint.2013.05.046

low cost, small electronegativity, and environmentally friendly characteristics. Hence, $LiMBO_3$ could be potential alternatives to phosphates by having the lower mass polyoxanion groups $(BO_3)^{3-}$ instead of $(PO_4)^{3-}$. Besides, $(BO_3)^{3-}$ polyoxanion can keep the advantage of the linking anion groups through the inductive effect of B–O bonds to give a high output potential and enhanced structural stability.

As reported by Legagneur for the first time [11], $LiMBO_3$ (M=Fe, Mn) can serve as lithium storage cathode material for lithium-ion batteries. However, they show low reversible capacity with only 0.02–0.04 Li per formula unit suffered from poor delithiation–lithiation kinetics. The slow kinetic behaviors are caused by inherent poor electronic and ionic conductivity with one-dimensional Li-diffusion pathways in the framework. Furthermore, $LiMBO_3$ is sensitive to air and moisture especially at high temperature, which can induce both Li loss from the crystal framework and partial oxidation of M^{2+} resulting in the formation of lithium-deficient but electrochemically inactive phase [12]. By coating the material with carbon layer and avoiding the exposure of the material to air and moisture, it can be found that the electronic conductivity and structural stability of $LiMBO_3$ are greatly improved [8–10,13]. As a result, a reversible capacity of 190 m Ah g^{-1} can be delivered by $LiFeBO_3$ in the working potential between 2.8 and 3.2 V at a rate of 0.05 C and the volume change during charge–discharge cycles is only 2% [12]. Although the lithium storage capacity of $LiFeBO_3$ is much higher than that of $LiFePO_4$, the operating potential is around 3.0 V resulting in lower energy density of the compound compared to $LiFePO_4$. In contrast, $LiMnBO_3$ reveals a theoretical output potential at around 4.6 V with the theoretical lithium storage capacity of 222 m Ah g^{-1}. Both the capacity and average operating potential are higher than those of $LiMnPO_4$. Moreover, compared to Co element used in commercial $LiCoO_2$ cathode material, Mn element shows lower cost, higher abundance and lower toxicity characteristics. Therefore, $LiMnBO_3$ can be promising cathode material for high capacity and high power lithium-ion batteries.

Unfortunately, it is difficult for hexagonal $LiMnBO_3$ synthesized by a conventional solid state method to display electrochemical activity even at a low rate of 0.02 C [11,14–16]. It is believed that intrinsically low ionic and electronic conductivities cause the poor electrochemical properties of $LiMnBO_3$. In this study, hexagonal $LiMnBO_3$ is prepared by a carbothermal reaction using carbon black as protective agent and carbon source. The crystal structure, particle morphology and electrochemical activity of hexagonal $LiMnBO_3$ are investigated as lithium storage material for lithium-ion batteries. It is expected that $LiMnBO_3$ embedded in conductive carbon matrices will improve the lithium storage capacity and decrease the charge–discharge polarization.

2. Experimental

2.1. Material preparation and characterization

In this work, $LiMnBO_3$ powders are prepared by a carbothermal reaction method using carbon black as a Mn^{2+} protective agent and conductive carbon matrix. To prepare $LiMnBO_3$ powders, a stoichiometric mixture of $LiOH \cdot H_2O$, $Mn(CH_3COO)_2 \cdot 4H_2O$, H_3BO_3 and carbon black are mixed by ball-milling and then pressed into pellets with the diameter of 20 mm. The as-prepared pellets are calcined in a tube furnace at 400 °C for 5 h and followed by 10 h at 750 °C under N_2 gas flow. The resulting pellets are crushed by ball-milling to obtain $LiMnBO_3$ powders.

The crystal structure and phase characterization of as-prepared $LiMnBO_3$ powders are characterized by X-ray diffraction (XRD) technique with Bruker AXS D8 Focus X-ray diffractometer using Cu Kα radiation (λ=0.15406 nm). Infrared (IR) active spectrum is collected by Shimadzu infrared spectrophotometer with the wavenumber between 400 and 2000 cm^{-1}. The surface morphology and particle size of sample are observed by JEOL S4800 scanning electron microscopy (SEM). The microstructure of $LiMnBO_3$ grains is carefully examined by JEOL 2010F high resolution transmission electron microscopy (HRTEM).

2.2. Electrode preparation and battery characterization

For lithium storage behaviors investigation, the $LiMnBO_3$ working electrodes are fabricated by mixing 80 wt% of $LiMnBO_3$ active materials, 10 wt% of conductive carbon black and 10 wt% of polyvinylidene fluoride binder in N-methylpyrrolidine to form a homogeneous slurry. The resulting slurry is coated on aluminum foil (for cathode) or copper foil (for anode) by a doctor blade method and dried at 120 °C for 12 h in a vacuum oven. The working electrodes are punched into disks with the diameter of 15 mm and pressed under a pressure of 40 MPa. The as-obtained electrodes show an average active layer thickness of 45 μm with average active material loading of 3.5 mg cm^{-2}.

For electrochemical characterization, homemade Swagelok-type $LiMnBO_3$/Li batteries are assembled by using $LiMnBO_3$ film as working electrode, metal lithium disk as counter electrode, Whatman glass fiber filter as separator, and 1 mol L^{-1} $LiPF_6$ dissolved in a mixture of ethylene carbonate and dimethyl carbonate (1:1, v/v) as electrolyte in an Etelux glove box filled with highly pure argon gas (O_2 and H_2O levels below 1 ppm). Before electrochemical characterization, all the $LiMnBO_3$/Li batteries are stored and aged for 12 h to ensure the working electrode saturate with electrolyte.

Galvanostatic charge–discharge cycling tests are carried out on Land CT 2001A multi-channel battery test system in a constant temperature cabinet (25 °C). Different cycling parameters are used in the experiment for cathode and anode testing. A current density of 5 mA g^{-1} is applied for cathode testing in the potential range of 2.5–4.8 V and a current density of 50 mA g^{-1} in the potential range of 0.0–3.0 V is used for anode testing. Cyclic voltammetry (CV) measurements are performed on CHI 1000B electrochemical workstation at a scan rate of 0.1 mV s^{-1} in the potential range 0.0–3.0 V and 2.5–4.8 V. The electrochemical impedance spectra (EIS) are collected on CHI 660D electrochemical workstation with an amplitude potential of 5 mV in the frequency range from 1 MHz to 100 mHz.

3. Results and discussion

The powder XRD pattern of as-prepared sample is shown in Fig. 1a. It is obvious that the diffraction peaks at 12.30°, 21.73°, 25.23°, 28.42°, 31.15°, 33.44°, 36.03°, 38.31°, 44.54°, 48.20°, 53.52°, 55.04°, 58.54° and 60.06° can be indexed to the (100), (110), (200), (001), (101), (210), (111), (300), (220), (301), (221), (311), (002) and (140) planes of hexagonal $LiMnBO_3$ (ICSD card no.94318), which is isotypic with the hexagonal form of $LiCdBO_3$. The lattice parameters of as-prepared hexagonal $LiMnBO_3$ are $a=8.1831$ Å and $c=3.1575$ Å, and the space group can be attributed to be P-6. All these data are in accordance with the results reported by other groups [11,14,15]. Besides, two diffraction peaks can be observed at 19.59° and 40.60°, which are attributed to the (110) and (040) lines of monoclinic $LiMnBO_3$ with the space group of C12/c1 (ICSD card no.200535). Based on previous report [10], it is known that hexagonal $LiMnBO_3$ is formed at high temperature but monoclinic $LiMnBO_3$ is obtained at low temperature. It suggests that monoclinic phase does not totally transform into hexagonal $LiMnBO_3$ during the carbothermal solid state reaction at 750 °C under N_2 gas flow.

Besides, additonal structure informtion can be delivered by IR spectrum as shown in Fig. 1b. It can be found that nine infrared active bands can be observed at 864, 800, 723, 711, 649, 630, 577, 456 and 419 cm^{-1}. As well-known, the infrared reflections from tetrahedral Li and Mn vibrational motions are always associated with the active bands in the frequency range between 100 and 500 cm^{-1}. Here, the infrared active bands at 456 and 419 cm^{-1} can be contributed to the vibrations of Li–O and Mn–O bonds. For $[BO_3]^{3-}$ group, the vibrations are split into four frequency ranges 1000–1450 cm^{-1} (ν_{as}, E''), 850–950 cm^{-1} (ν_s, A'), 650–850 cm^{-1} (γ, A''), and 500–650 cm^{-1} (δ, E'), corresponding to four different types of vibrations of trigonal $[BO_3]^{3-}$ with D_{3h} symmetry [17,18]. As shown in Fig. 1b, in-plane deformation modes (577, 630 and 649 cm^{-1}), out-of-plane bending vibrations (711, 723 and 800 cm^{-1}) and symmetric stretching (864 cm^{-1}) of B–O bonds appear in the IR spectrum of hexagonal $LiMnBO_3$.

According to the structure information revealed by XRD and IR in Fig. 1, the crystal structure of $LiMnBO_3$ can be built by trigonal MnO_5 bipyramids and BO_3 planers to form three-dimensional $[MnBO_3]$ framework. As shown in Fig. 2, the trigonal MnO_5 bipyramid is formed by manganese atom coordinating with five oxygen atoms and BO_3 planars are built by boron atom coordinating with three oxygen atoms to form a three- or four-fold coordination environment. Each trigonal MnO_5 bipyramid shares two opposite edges of its square base with two adjacent pyramids and BO_3 planars link three chains by corner sharing to form a hexagonal framework of $LiMnBO_3$. The low energy pathway for lithium ion diffusion is one-dimensional in the hexagonal structure and lithium ion needs to migrate through the faces of adjacent oxygen tetrahedras during charge–discharge process.

The surface morphology and particle size of as-preprared hexagonal $LiMnBO_3$ are shown in Fig. 3. It is clear that hexagonal $LiMnBO_3$ sample displays spherical shape with the particle size distribution bewteen 0.2 and 1.0 μm, and these

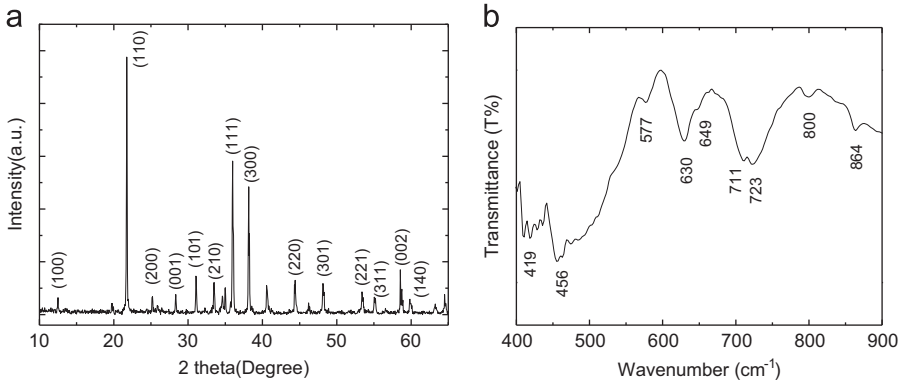

Fig. 1. XRD and IR patterns of hexagonal $LiMnBO_3$.

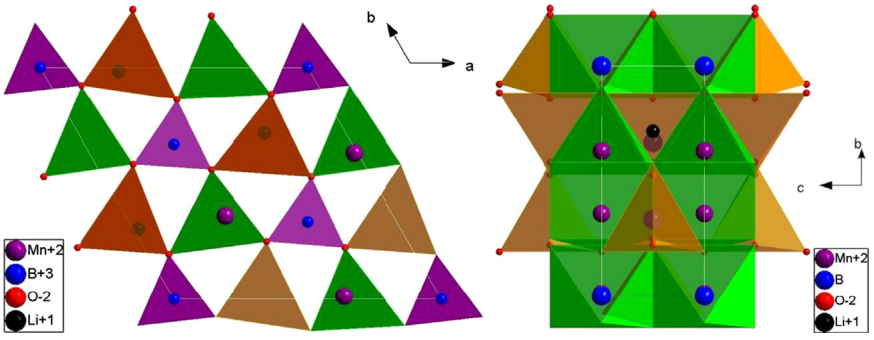

Fig. 2. The crystal structure of hexagonal $LiMnBO_3$.

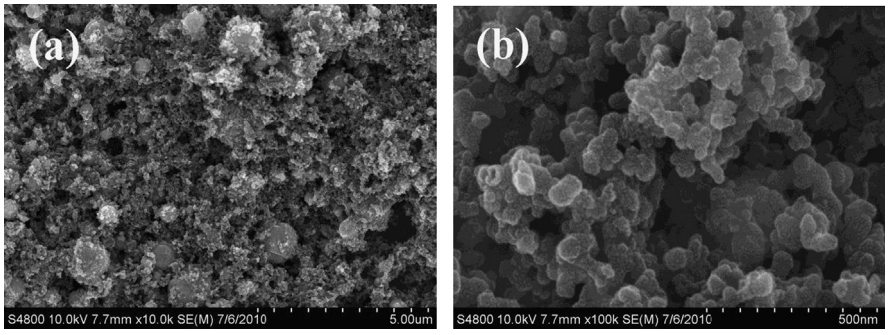

Fig. 3. SEM images of hexagonal $LiMnBO_3$.

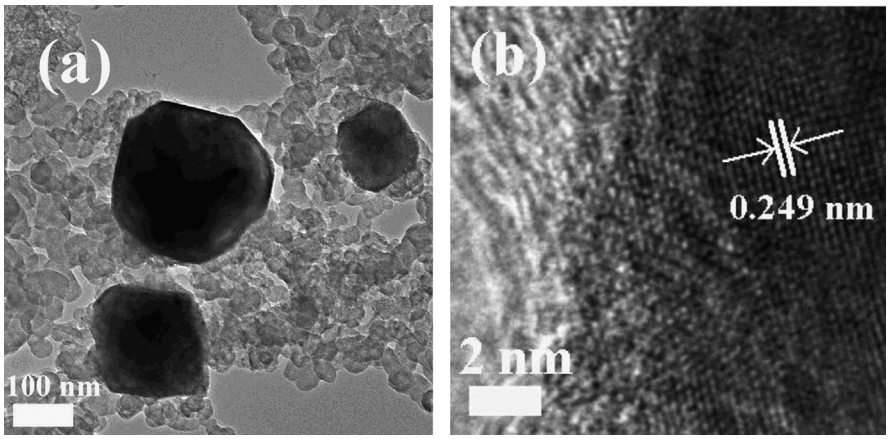

Fig. 4. HRTEM images of hexagonal $LiMnBO_3$.

active particles are embedded in the carbon black matrix. The conductive three-dimensional carbon network will greatly improve the electronic conductivity of pristine $LiMnBO_3$ (10^{-7}–10^{-8} S cm^{-1}). The fine microstructure of $LiMnBO_3$ grains is exhibited in Fig. 4. Based on the HRTEM images, the lattice distance is measured to be 0.249 nm for the index of (111) plane of hexagonal $LiMnBO_3$, which is also in agreement with the XRD and IR results.

Fig. 5 shows the lithium storage behaviors of hexagonal $LiMnBO_3$ in the potential range 0.0–3.0 V and 2.5–4.8 V. For the sample cycled in 2.5–4.8 V, hexagonal $LiMnBO_3$ is used as cathode material for lithium-ion batteries. In contrast, hexagonal $LiMnBO_3$ becomes an anode material by cycling in 0.0–3.0 V. Here, the CV curves obtained in different potential ranges are displayed in Fig. 5. It is obvious that only one oxidation peak can observed at around 4.75 V in the initial anodic scan and a weak reduction peak can be detected at 4.20 V in the reverse cathodic scan. However, it is difficult to observe the redox couples in the following scans. It indicates that lithium ions can extract from the structure of hexagonal $LiMnBO_3$ in the charge process. However, most lithium ions can not re-insert into the empty sites in the hexagonal structure between 2.5 and 4.8 V. By using hexagonal $LiMnBO_3$ as anode material, it can be found that there are two reduction peaks appeared at 0.53, 0.10 V and two reverse oxidation peaks reappeared at 0.20, 1.05 V in the first cycle. Except for the shift of reduction peak from 0.53 to 0.68 V, the subsequent CV curves are almost overlapped with the initial one, which suggests that the lithiation–delithiation behaviors of hexagonal $LiMnBO_3$ as anode material are high degree reversible.

The charge–dischage curves and corresponding cyclic performance of hexagonal $LiMnBO_3$ in the potential range 2.5–4.8 V and 0.0–3.0 V are shown in Fig. 6. The charge–discharge behaviors and shapes of our sample are similar to those in the reported literatures [13–16]. The hexagonal $LiMnBO_3$ cathode shows a delithiation plateau at about 4.76 V with an initial charge capacity of 148.4 m Ah g^{-1}, corresponding to 0.668 Li delithiation per formula, which is much higher than the value of 0.340 Li (75.5 m Ah g^{-1}) reported by Chen [15]. The reverse discharge process displays an initial lithiation capacity of 27.4 m Ah g^{-1}, corresponding to 0.123 Li per formula storage in the structure. This value is lower than the lithiation capacity of 40–50 m Ah g^{-1} reported by Chen and Lee [15,16]. However, most lithium storage capacity comes from electrolyte decomposition with the working potential below 2.0 V in these literatures. In this paper, the sample is cycled in the potential range between 2.5 and 4.8 V. Therefore, extra capacity from side reactions below 2.5 V can be excluded. After 20 cycles, the reversible discharge capacity is only 8.9 m Ah g^{-1}, which is much lower than the data delivered by reported monoclinic $LiMnBO_3$ cathode material [9,10,14]. Higher activation barriers of lithium ion diffusion in hexagonal $LiMnBO_3$ than that in monoclinic $LiMnBO_3$ can explain the difference in the electrochemical performance between the monoclinic and hexagonal phases [14]. For hexagonal $LiMnBO_3$ anode, it shows two lithiation plateaus

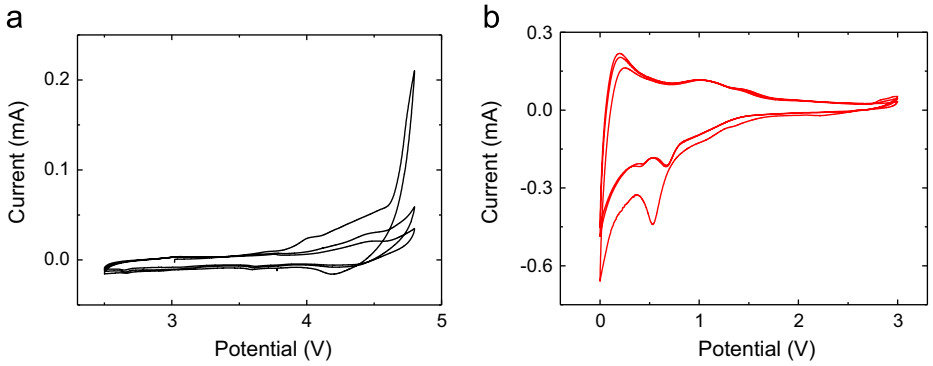

Fig. 5. CV curves of hexagonal $LiMnBO_3$: (a) 2.5–4.8 V; (b) 0.0–3.0 V.

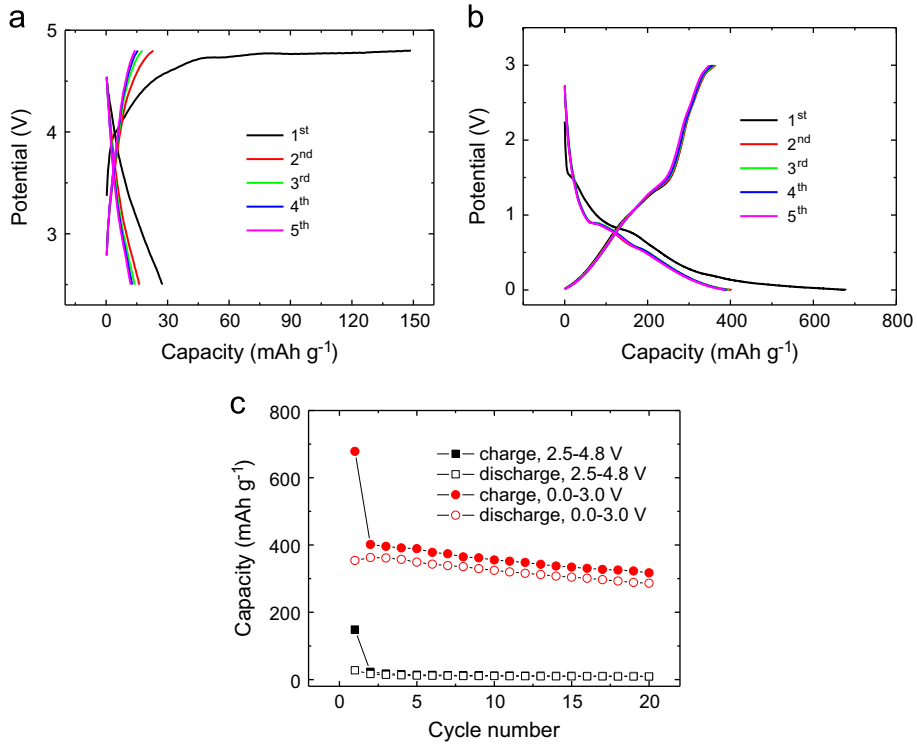

Fig. 6. Charge–discharge curves and corresponding cycling properties of hexagonal $LiMnBO_3$: (a, c) 2.5–4.8 V; (b, c) 0.0–3.0 V.

at 0.76 and 0.06 V with the initial discharge capacity of 678.3 m Ah g^{-1}, corresponding to 3.055 Li per formula storage in hexagonal $LiMnBO_3$. The value is much higher than the theoretical one (222 mAh g^{-1}) of $LiMnBO_3$ cathode material as reported in the literatures [9–11,14–16]. Therefore, it may have a new lithium storage mechanism by using hexagonal $LiMnBO_3$ as anode material, which shows a higher theoretical capacity on the supposition of formation of new lithiation products. In the reserve charge process, two slopes can be observed in the potential range 0.0–1.45 V and 1.45–3.0 V, and a corresponding delithiation capacity is about 353.9 mAh g^{-1}. After 20 cycles, the reversible charge capacity for hexagonal $LiMnBO_3$ anode is 286.4 m Ah g^{-1}, corresponding to 1.290 Li per formula delithiation from the structure. The capacity retention of hexagonal $LiMnBO_3$ anode is 80.9% after 20 repeated cycles. It suggests that the host structure of hexagonal $LiMnBO_3$ anode may be retained upon repeated delithiation–lithiation processes.

To display the electrochemically inactivity and capacity loss of hexagonal $LiMnBO_3$ during cycles, EIS, ex-situ XRD and ex-situ IR techniques are used in the experiment. Fig. 7 shows the EIS spectra of hexagonal $LiMnBO_3$ at different lithiation and delithiation states in different potential ranges. The detailed electrochemical impedance parameters are refined by ZView software and displayed in Table 1. EIS plots are sensitive to the evolutions of components in the electrode. Using as cathode material, hexagonal $LiMnBO_3$ shows the increase in electrolyte resistance from 7.16 to 17.58 Ω and the increase in charge transfer resistance from 19.43 to 178.6 Ω upon a charge process to 4.8 V. The increase of electrolyte resistance is attributed to the electrolyte oxidation decomposition at high operating potential. The increase of charge transfer

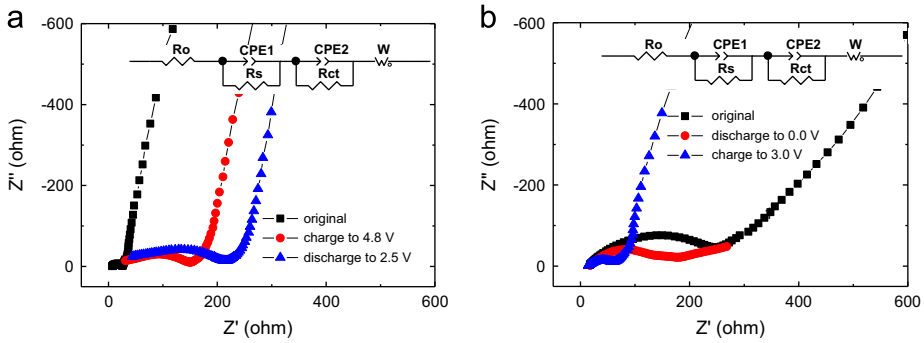

Fig. 7. EIS spectra of hexagonal $LiMnBO_3$ at different delithiation–lithiation states: (a) 2.5–4.8 V; (b) 0.0–3.0 V.

Table 1
Electrochemical impedance parameters of hexagonal $LiMnBO_3$ at different delithiation–lithiation states.

Sample	R_o (Ω)	R_s (Ω)	CPE1 (μF)	R_{ct} (Ω)	CPE2 (μF)
$LiMnBO_3$-cathode	7.16	0	0	19.43	4.21E-5
$LiMnBO_3$-4.8 V	17.58	165.1	1.31E-4	178.6	5.42E-5
$LiMnBO_3$-2.5 V	19.27	252	1.05E-4	385.70	2.65E-5
$LiMnBO_3$-anode	15.33	0	0	266.3	4.54E-5
$LiMnBO_3$-0.0 V	17.17	143.2	9.25E-5	175.4	1.09E-4
$LiMnBO_3$-3.0 V	13.52	60.42	2.11E-4	90.32	3.06E-4

resistance is probably attributed to the formation of thick solid electrolyte interphase (SEI) film on the surface of active materials [19]. With a reverse discharge to 2.5 V and a discharge capacity of 27.4 m Ah g^{-1}, the charge transfer resistance maintains a gradual increase as shown in Fig. 7a. Therefore, it is thought that the degradation of electrolyte and the increase of SEI film still take place in the discharge process. By using as anode material, hexagonal $LiMnBO_3$ shows a continuous decrease in charge transfer resistance from 266.3 to 90.32 Ω. For comparison, no obvious change can be observed for electrolyte resistance (around 15 Ω). In Nyquist plot, two semicycles can be observed when the electrode is dicharged to 0.0 V. The new semicycle is attributed to the formation of SEI film via electrolyte reduction decomposition [20]. Although SEI film is formed on the surface, the charge transfer resistance reveals an obvious decrease from 266.3 to 175.4 Ω. The decrease of charge transfer resistance can be explained by an increase in the contact area between active material and the SEI film as shown in Fig. 8. It reveals that the spherical $LiMnBO_3$ particles pulverize into smaller bulks after repeated cycles in 0.0–3.0 V. As a result, the kinetics of delithiation–lithiation process is fast for hexagonal $LiMnBO_3$ anode.

The ex-situ XRD and ex-situ IR patterns of hexagonal $LiMnBO_3$ in the charged and discharged states are depicted in Figs. 9 and 10. The $LiMnBO_3$ electrodes for ex-situ observation are extracted by disassembling the $LiMnBO_3$/Li batteries, followed by XRD and IR measurements. The electrodes for ex-situ XRD are prepared in the Ar-filled glove box and covered with a polymer film to avoid the exposure to air and moisture. The samples for ex-situ IR are washed with dimethyl carbonate, vacuumed overnight, and then mixed with KBr powder to form pellets before use.

Seen from Fig. 9a, it can be found that the main diffraction peaks of hexagonal $LiMnBO_3$ cathode are maintained but show slight shift to higher angles after a full delithiation process to 4.8 V with 0.668 Li delithiation per formula. Furthermore, a long flat delithiation plateau appears in the charge process as shown in Fig. 6a, indicating the lithium storage mechanism of hexagonal $LiMnBO_3$ related to a topotactic lithiation–delithiation process to form new phase with isostructure of the pristine sample. This phenomenon is similar to the two-phase mechanism reported from micro-sized $LiFePO_4$ and $Li_4Ti_5O_{12}$ samples [5,21–23]. For comparison, a solid solution lithiation–delithiation mechanism with slope charge–discharge curves can be observed in the nano-sized hexagonal $LiMnBO_3$ sample (20–80 nm) as reported by Afyon et al. [9]. In the reverse discharge process, all the diffraction peaks move back but the relative intensities can not recover as high as those of the pristine sample. This result is in accordance with the electrochemical data for only 0.123 Li per formula re-storage in the structure during the discharge process with the irreversible capacity of 0.545 Li per formula unit.

Although 3.055 Li per formula can be stored during the initial discharge process, the crystal structure of hexagonal $LiMnBO_3$ anode material does not totally collapse as shown in Fig. 9b. Compared with the pristine XRD pattern, it is clear that the diffraction peak at 40.5° indexed to impurity monoclinic $LiMnBO_3$ disappears for lithiation XRD pattern (Fig. 9b) and other diffraction peaks (such as 25.0 and 34.6°) of hexagonal $LiMnBO_3$ do not disappear and merely become very weak after a discharge to 0.0 V. Therefore, it is impossible for hexagonal $LiMnBO_3$ to decompose and form the products of LiB, Li_2O and Mn after a discharge process to

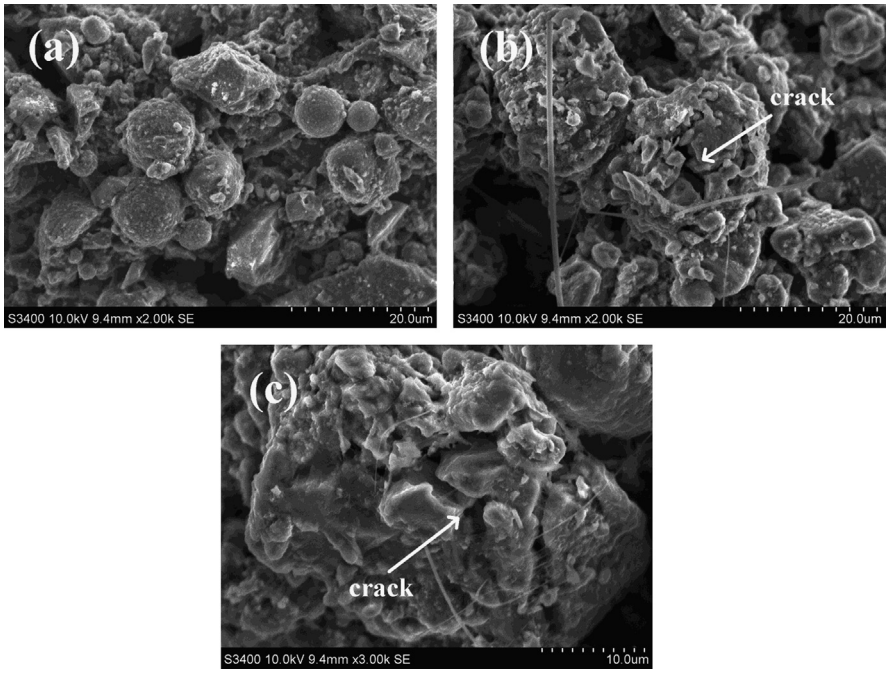

Fig. 8. SEM images of hexagonal $LiMnBO_3$ before (a) and after cycles (b, c) in 0.0–3.0 V.

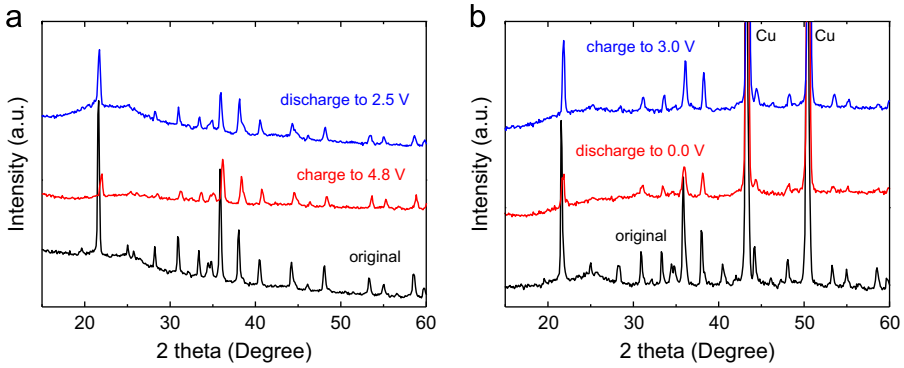

Fig. 9. Ex-situ XRD patterns of hexagonal $LiMnBO_3$ at different delithiation–lithiation states: (a) 2.5–4.8 V; (b) 0.0–3.0 V.

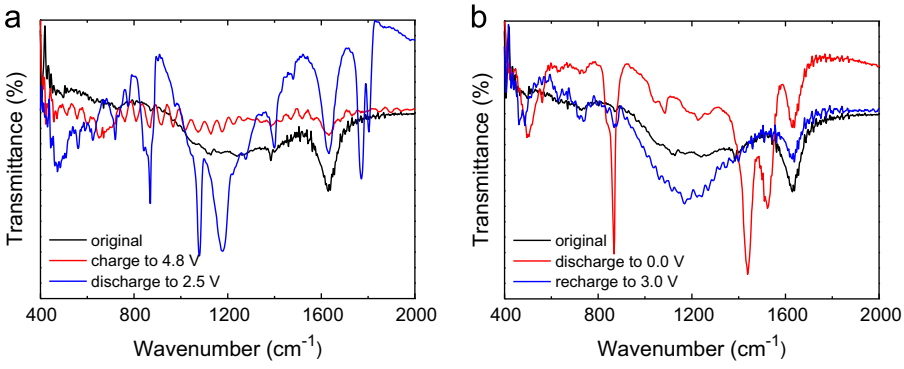

Fig. 10. Ex-situ IR spectra of hexagonal $LiMnBO_3$ at different delithiation–lithiation states: (a) 2.5–4.8 V; (b) 0.0–3.0 V.

0.0 V. It is quite different from other cathode materials (such as $LiCoO_2$, $LiMn_2O_4$ and $LiFePO_4$) as described by our previous papers [24,25]. By using as anode material, hexagonal $LiMnBO_3$ anode material exhibits a quasi-symmetrical shift in the diffraction peaks as shown in Fig. 9b. It can be seen that the major diffraction peaks shift slightly between lithiation and delithiation states. Moreover, the SEM images shown in Fig. 8b and c indicate that the active particles pulverize and

become smaller grains upon electrochemical cycling. As a result, the contact area between active particles and SEI film increases and results in the decrease of charge transfer resistance as shown in Fig. 7b and Table 1. This observation also indicates that there has no completely structural breakdown occurring after full lithiation–delithiation process. Moreover, the quasi-symmetrical shift of Bragg positions indicates a reversible lithiation–delithiation reaction during charge–discharge process. This result is in good agreement with the excellent cycling properties of hexagonal $LiMnBO_3$ anode material as shown in Fig. 6b and c.

Further structure and surface variations can be observed by ex-situ IR technique. As shown in Fig. 10a, the in-plane deformation mode of B-O bonds shows a blue-shift from 630 to 653 cm^{-1} upon charging and displays a reversible red-shift from 653 to 626 cm^{-1} upon dischargeing. It indicates that the strcutural evolution of hexagonal $LiMnBO_3$ cathode is almost reversible by cycling in the potential range between 2.5 and 4.8 V. Besides, new bands located at 1805, 1769, 1482, 1401, 1177 and 1079 cm^{-1} in the lithiation pattern can be contributed to dimethyl carbonate, Li_2CO_2, $ROCO_2Li$ in SEI film [26–28], which can explain the gradual increase of charge transfer resistance upon a discharge process to 2.5 V as shown in Fig. 7a. For hexagonal $LiMnBO_3$ anode as shown in Fig. 10b, no evolution of the bands at 873, 729 and 630 cm^{-1} can be detected but the peaks in the frequency range 450–550 cm^{-1} reveal great variation during the charge–discharge process. It can be found that the characteristic band at 577 cm^{-1} shows a red-shift to 563 cm^{-1} upon a discharge process to 0.0 V and then disappears. Similarly, the vibration from Li motion in tetrahedras splits into two new bands centered at 486 and 460 cm^{-1} after a charge process to 3.0 V, suggesting the structural difference between the pristine hexagonal $LiMnBO_3$ and the charged sample. Furthermore, the new bands appeared at 1523, 1438, 1267, 1227, 1182, 1083 and 1043 cm^{-1} in the discharged sample can be also responsible for the formation of SEI film on anode [26–30]. In contrast, the disappearance of infrared bands at 1523 and 1438 cm^{-1} after a charge process to 3.0 V indicates the partial decomposition of surface film, which is in agreement with the decrease of resistance of SEI film as shown in Table 1. Besides, the difference in the active bands of the SEI films on cathode and anode materials indicates the different deposited products formed from different electrochemical reactions.

4. Conclusion

In this work, we prepare hexagonal $LiMnBO_3$ lithium storage host materials by a high-temperature solid state reaction method. The as-prepared samples are spherical particles with particle size between 0.2 and 1.0 μm and surrounded by conductive carbon black. The nano-sized carbon black prevents the growth of active particles, leading to the formation of $LiMnBO_3$/C. On the other hand, the conductive carbon black provides good electronic bridges between particles, which improve the electronic conductivity of the pristine sample. In the experiment, the as-prepared hexagonal $LiMnBO_3$ samples are tested respectively as cathode and anode materials for lithium-ion batteries. It can be found that hexagonal $LiMnBO_3$ shows poor electrochemical lithium storage capability as cathode material in the potential range 2.5–4.8 V. For comparison, hexagonal $LiMnBO_3$ anode can take 3.055 Li per formula unit storage in the structure and yields a reversible charge capacity of 286.4 m Ah g^{-1} after 20 cycles in the potential range 0.0–3.0 V.

Acknowledgments

This work is sponsored by the National 863 Program (2013AA050901), National Natural Science Foundation of China (No. 51104092) and Qianjiang Talent Project of Zhejiang Province (2011R10089). The work is also supported by K.C. Wong Magna Fund in Ningbo University, Open Foundation of State Key Laboratory of Materials Processing and Die & Mould Technology (2012-P01), Open Foundation of State Key Laboratory of Electronic Thin Films and Integrated Devices (KFJJ201209) and Open Foundation of State Key Laboratory Breeding Base of Green Chemistry-Synthesis Technology (GCTKF2012002).

References

[1] A.K. Padhi, K.S. Nanjundaswamy, J.B. Goodenough, Phospho-olivines as positive-electrode materials for rechargeable lithium batteries, Journal of the Electrochemical Society 144 (1997) 1188–1194.
[2] X. Xia, Z.X. Wang, L.Q. Chen, Regeneration and characterization of Air-Oxidized $LiFePO_4$, Electrochemistry Communications 10 (2008) 1442–1444.
[3] W. Dreyer, J. Jamnik, C. Guhlke, R. Huth, J. Moškon, M. Gaberščcek, The thermodynamic origin of hysteresis in insertion batteries, Nature Materials 9 (2010) 448–453.
[4] S. Nishimura, G. Kobayashi, K. Ohoyama, R. Kanno, M. Yashima, A. Yamada, Experimental visualization of lithium diffusion in Li_xFePO_4, Nature Materials 7 (2008) 707.
[5] C. Delmas, M. Maccario1, L. Croguennec1, F. Le Cras, F. Weill, Lithium deintercalation in $LiFePO_4$ nanoparticles via a domino-cascade model, Nature Materials 7 (2008) 665–671.
[6] Y. Janssen, D.S. Middlemiss, S.H. Bo, C.P. Grey, P.G. Khalifah, Structural modulation in the high capacity battery cathode material $LiFeBO_3$, Journal of America Chemistry Society 134 (2012) 12516–12527.
[7] S.H. Bo, F. Wang, Y. Janssen, D.L. Zeng, K.W. Nam, W.Q. Xu, L.S. Du, J. Graetz, X.Q. Yang, Y.M. Zhu, J.B. Parise, C.P. Grey, P.G. Khalifah, Degradation and (de)lithiation processes in the high capacity battery material $LiFeBO_3$, Journal of Materials Chemistry 22 (2012) 8799–8809.
[8] P. Barpanda, Y. Yamashita, Y. Yamada, A. Yamada, High-throughput solution combustion synthesis of high-capacity $LiFeBO_3$ cathode, Journal of the Electrochemical Society 160 (2013) A3095–A3099.
[9] S. Afyon, D. Kundu, F. Krumeich, R. Nesper, Nano $LiMnBO_3$, a high-capacity cathode material for li-ion batteries, Journal of Power Sources 224 (2013) 145–151.
[10] S.L. Li, L.Q. Xu, G.D. Li, M. Wang, Y.J. Zhai, In-situ controllable synthesis and performance investigation of carbon-coated monoclinic and hexagonal $LiMnBO_3$ composites as cathode materials in lithium-ion batteries, Journal of Power Sources 236 (2013) 54–60.
[11] V. Legagneur, Y. An, A. Mosbah, R. Portal, A. Le Gal La Salle, A. Verbaere, D. Guyomard, Y. Piffard, $LiMBO_3$ (M=Mn, Fe, Co): synthesis, crystal structure and lithium deinsertion/insertion properties, Solid State Ionics 139 (2001) 37–46.

[12] A. Yamada, N. Iwane, Y. Harada, S. Nishimura, Y. Koyama, I. Tanaka, Lithium iron borates as high-capacity battery electrodes, Advanced Materials 22 (2010) 3583–3587.
[13] V. Aravindan, M. Umadevi, Synthesis and characterization of novel $LiFeBO_3$/C cathodes for lithium batteries, Ionics 18 (2012) 27–30.
[14] J.C. Kim, C.J. Moore, B. Kang, G. Hautier, A. Jain, G. Ceder, Synthesis and electrochemical properties of monoclinic $LiMnBO_3$ as a Li intercalation material, Journal of the Electrochemical Society 158 (2011) A309–A315.
[15] L. Chen, Y.M. Zhao, X.N. An, J.M. Liu, Y.Z. Dong, Y.H. Chen, Q. Kuang, Structure and electrochemical properties of $LiMnBO_3$ as a new cathode material for lithium-ion batteries, Journal of Alloys and Compounds 494 (2010) 415–419.
[16] Y.S. Lee, H. Lee, Electrochemical properties of $LiMnBO_3$ as a potential cathode material for lithium batteries, Journal of Ceramic Processing Research 13 (2012) s237–s240.
[17] A. Belkebir, P. Tarte, A. Rulmont, B. Gilbert, Synthesis, structural and vibrational analysis of $LiMBO_3$ orthoborates (M=Mg, Co, Zn), New Journal of Chemistry 20 (1996) 311–316.
[18] S. Filatov, Y. Shepelev, R. Bubnova, N. Sennova, A.V. Egorysheva, Y.F. Kargin, The study of $Bi_3B_5O_{12}$: synthesis, crystal structure and thermal expansion of oxoborate $Bi_3B_5O_{12}$, Journal of Solid State Chemistry 177 (2004) 515–522.
[19] C.S. Wang, A.J. Appleby, F.E. Little, Electrochemical impedance study of initial lithium ion intercalation into graphite powders, Electrochimica Acta 46 (2001) 1793–1813.
[20] J.S. Gnanaraj, R.W. Thompson, S.N. Iaconatti, J.F. DiCarlo, K.M. Abraham, Formation and growth of surface films on graphitic anode materials for Li-ion batteries, Electrochemical and Solid-State Letters 8 (2005) A128–A132.
[21] R. Malik, F. Zhou, G. Ceder, Kinetics of non-equilibrium lithium incorporation in $LiFePO_4$, Nature Materials 10 (2011) 587–590.
[22] J. Shu, Electrochemical behavior and stability of $Li_4Ti_5O_{12}$ in a broad voltage window, Journal of Solid State Electrochemistry 13 (2009) 1535–1539.
[23] J.W. Shin, K.Y. Chung, J.H. Ryu, I.W. Park, D.H. Yoon, Effects of Li/Ti ratios on the electrochemical properties of $Li_4Ti_5O_{12}$ examined by time-resolved X-ray diffraction, Applied Physics A 107 (2012) 769–775.
[24] J. Shu, M. Shui, F.T. Huang, Y.L. Ren, Q.C. Wang, D. Xu, L. Hou, A New, Look at lithium cobalt oxide in a broad voltage range for lithium ion batteries, Journal of Physical Chemistry C 114 (2010) 3323–3328.
[25] J. Shu, M. Shui, D. Xu, D.J. Wang, Y.L. Ren, S. Gao, A comparative study of over-discharge behaviors of cathode materials for lithium-ion batteries, Journal of Solid State Electrochemistry 216 (2012) 819–824.
[26] D. Aurbach, M.L. Daroux, P.W. Faguy, E. Yeager, Identification of surface films formed on lithium in propylene carbonate solutions, Journal of the Electrochemical Society 134 (1987) 1611–1620.
[27] J. Shu, Study of the interface between $Li_4Ti_5O_{12}$ electrodes and standard electrolyte solutions in 0.0–5.0 V, Electrochemical and Solid-State Letters 11 (2008) A238–A240.
[28] D. Aurbach, B. Markovsky, I. Weissman, E. Levi, Y. Ein-Eli, On the correlation between surface chemistry and performance of graphite negative electrodes for Li ion batteries, Electrochimica Acta 45 (1999) 67–86.
[29] D. Aurbach, B. Markovsky, M.D. Levi, E. Levi, A. Schechter, M. Moshkovich, Y. Cohen, New insights into the interactions between electrode materials and electrolyte solutions for advanced nonaqueous batteries, Journal of Power Sources 81–82 (1999) 95–111.
[30] D. Aurbach, B. Markovsky, A. Schechter, Y. Ein-Eli, Y. Cohen, A Comparative study of synthetic graphite and Li electrodes in electrolyte solutions based on ethylene carbonate-dimethyl carbonate mixtures, Journal of the Electrochemical Society 143 (1996) 3809–3820.